Nanoscale

Measurements of Aptamer-Protein Binding Kinetics Using Graphene Field-Effect Transistors

Journal:	*Nanoscale*
Manuscript ID	NR-ART-04-2019-002797.R1
Article Type:	Paper
Date Submitted by the Author:	06-Jun-2019
Complete List of Authors:	Wang, Xuejun; Columbia University, Mechanical Engineering ; Fudan University, Macromolecular Science Hao, Zhuang; Columbia University, Mechanical Engineering; Harbin Institute of Industry Olsen, Tim; Columbia University, Mechanical Engineering Zhang, Wenjun; University of Saskatchewan Lin, Qiao; Columbia University, Dept of Mechanical Engineering

Measurements of Aptamer-Protein Binding Kinetics Using Graphene Field-Effect Transistors

Received 00th January 20xx,
Accepted 00th January 20xx

DOI: 10.1039/x0xx00000x

Xuejun Wang[a,b], Zhuang Hao[a], Timothy R. Olsen[a], Wenjun Zhang[c], Qiao Lin*[a]

Quantifying interactions between biomolecules subject to various environmental conditions is essential for applications such as drug discovery and precision medicine. This paper presents an investigation of the kinetics of environmentally dependent biomolecular binding using an electrolyte-gated graphene field-effect transistor (GFET) nanosensor. In this approach, biomolecular binding occurring on and in the vicinity of a graphene surface induces a change in carrier concentration, whose resulting conductance change is measured. This allows a systematic study of the kinetic properties of the binding system. We apply this approach to the specific binding of human immunoglobulin E (IgE), an antibody involved in parasite immunity, with an aptamer at different ionic strengths (Na^+ and Mg^{2+}) and temperatures. Experimental results demonstrate increased-rate binding kinetics at higher salt-ion concentrations and temperatures. In particular, the divalent cation Mg^{2+} yields more pronounced changes in the conformational structure of the aptamer than the monovalent cation Na^+. In addition, the dissociation of the aptamer complex at room temperature is ofound to be characterized by large unfavorable changes in the activation enthalpy and entropy.

1. Introduction

Characterizing the kinetics and thermodynamics of biomolecular binding systems is essential to elucidating intermolecular interactions. Kinetic measurements of biomolecular interactions currently rely on fluorescent, gravimetric and optical methods.[1-3] Among these, fluorescent methods allow direct binding measurement and enable binding assessment in unconventional materials (e.g. on cell surfaces), but may be susceptible to measurement inaccuracies because of direct modifications of ligands with labeling probes. Such modifications are inconvenient, may interfere with the intended biomolecular binding, and may not be applicable to molecules that are not amenable to fluorescent probe attachments. Gravimetric methods such as the quartz crystal microbalance (QCM), and optical methods such as surface plasmon resonance (SPR), are label-free but strongly depend on the size of target molecules, and thus are not well suited to low-molecular-weight molecules. Moreover, QCM and SPR typically require bulky and expensive instruments and have limited throughput.

Miniaturized label-free measurement systems that use microscale and nanoscale functional materials provide an attractive avenue for studies of biomolecular binding.[4-7] In particular, graphene, a two-dimensional nanomaterial, has many unique properties for label-free biomolecular interaction measurements. For example, in graphene field-effect transistor (GFET) sensors, changes in charge distribution in the close vicinity of the graphene surface result in measurable changes in the bulk electrical conductance of the graphene, which can be exploited to characterize both equilibrium and kinetic properties of molecular binding systems. Existing GFET sensors, while having been used extensively for detection, under equilibrium conditions, of target species such as DNA,[8] proteins,[9] and bacteria,[10] have not been systematically employed as a tool to characterize biomolecular binding kinetics. Although a limited number of studies have used GFET sensors to demonstrate real-time quantification of binding kinetics for proteins,[10,11] these measurements were obtained with small volumes of aqueous samples exposed to the open atmosphere. Thus, these techniques may be susceptible to external disturbances such as evaporation and could hence be inaccurate. Additionally, these studies used stopped-flow measurements, which may be susceptible to mass transfer-limited kinetic binding processes.[12] Recently, GFET was used for real-time monitoring of DNA hybridization kinetics, with an attempt to circumvent the evaporation and mass transfer limitations by using an integrated microfluidic system, although the use of an out-of-plane gate electrode did not allow the intended miniaturization of the measurement system.[13] In addition, a detailed understanding of biomolecular binding under varying environmental conditions such as ionic strength and temperature, which is important to applications such as drug discovery and precision medicine,[14] has not been pursued with graphene nanosensors.

This paper exploits GFET sensors for the systematic characterization of biomolecular binding, emphasizing kinetic measurements under varying conditions of ionic strength and temperature. This use of GFET sensors as a tool for biomolecular binding characterization represents a new application that offers a number of unique advantages. First, the high sensitivity and low noise levels of GFET nanosensors offer a high signal-to-noise ratio in binding measurements. As a result, this approach is more reliable and sensitive and does not require additional signal-correction components that are commonly used in conventional methods such as SPR. Second, because of the high carrier mobility of graphene, GFET sensors offer a rapid response. Compared to existing methods (e.g., SPR) with time responses on the order of seconds, our approach offers improvements by an order of magnitude (70 milliseconds or less in time response) and is well suited to biomolecular systems with fast binding kinetics. Third, because of the small thermal mass of GFET nanosensors, our approach is appropriate for measurements of temperature-dependent binding kinetics; in contrast, existing SPR and ITC methods either involve relatively larger thermal masses or are not effective for systems with low binding enthalpies. Effects of evaporation, which can be

[a] Department of Mechanical Engineering, Columbia University, New York, NY 10027, USA.
[b] State Key Laboratory of Molecular Engineering of Polymers, Department of Macromolecular Science, Fudan University, Shanghai, 200438, China.
[c] Department of Mechanical Engineering, University of Saskatchewan, Saskatoon, S7N 5A9, Canada.
*corresponding author: qlin@columbia.edu
Electronic Supplementary Information (ESI) available: See DOI:10.1039/x0xx00000x

even more pronounced at elevated temperatures, are minimized using closed-volume measurements inside a microfluidic channel. Finally, with a one-step electrical readout, the GFET nanosensors afford convenient measurements and instrumentation simplifications, while also facilitating miniaturization of the measurement system.

The GFET-based binding measurement approach is demonstrated through kinetic characterization of the binding of human immunoglobulin E (IgE), an antibody involved in parasite immunity that was used as a representative analyte, to a specific aptamer (D17.4). Time-resolved measurements are performed under differing environmental conditions, such as temperature as well as Na^+ and Mg^{2+} ion concentrations. Results from the measurements provide systematic insights into kinetic aptamer-IgE binding characteristics, and also allow the determination of thermodynamic properties, such as enthalpy, entropy, and free energy changes of activation of the binding system. These results demonstrate the potential use of graphene affinity nanosensors as an innovative tool for measuring the binding kinetics and thermodynamic properties of biomolecular systems.

2. Experimental

2.1 Principle and Design

The nanosensor is an electrolyte-gated GFET (Fig. 1a) with an embedded gate electrode and a temperature sensor (Fig. 1b). An electrical double layer (EDL) formed at the interface of the graphene and solution serves as the gate capacitor. An applied drain-source bias (V_{ds}) generates a current (I_{ds}) through a graphene conducting channel that connects drain and source electrodes (Fig. 1c), and this drain current can be tuned by altering gate voltage (V_g). Graphene is immobilized with aptamer molecules that are used for target recognition. Binding of protein and aptamer molecules results in a large change in the conformational structure of the aptamer, which brings the target to the close vicinity of the graphene surface and induces a change in the carrier concentration of the graphene. This results in a graphene conductance change, which is measured to determine the protein concentration. The association and dissociation between the aptamer and the protein generate a time-varying changes in the drain-current, which is measured to study the aptamer-IgE binding.

2.2 Materials

Graphene was synthesized via chemical vapor deposition (CVD). Polydimethylsiloxane (PDMS, Sylgard-184) was purchased from Dow Corning (Midland, MI) for fabricating the PDMS microfluidic channel. 1-pyrenebutanoic acid succinimidyl ester (PASE) linker and phosphate buffered saline (PBS) were purchased from Thermo Fisher Scientific (Waltham, MA). Immunoglobulin E (IgE) protein was purchased from Athens Research and Technology (Athens, GA). The 5'-amino modified DNA aptamer D17.4 (5'-GCG CGG GGC ACG TTT ATC CGT CCC TCC TAG TGG CGT GCC CCG CGC-3') for IgE was synthesized and purified by Integrated DNA Technologies (Coralville, IA). Dimethylformamide, ethanolamine and other related chemicals used in functionalization and experiments were obtained from Sigma-Aldrich (St. Louis, MO).

2.3 Device Fabrication and Surface Functionalization

The device was fabricated using standard micro and nanofabrication techniques shown in Fig. S1 in Supplementary Information (SI). Graphene was transferred to a 285-nm SiO_2-coated Si substrate following a reported protocol.[8] Source, drain and gate electrodes along with the on-chip temperature sensor (5/50 nm Cr/Au) were subsequently fabricated using photolithography, and the graphene was further patterned to define the sensing region through oxygen plasma etching. In addition, a microfluidic channel made of polydimethylsiloxane (PDMS) (1 mm in width and 20 μm in height) was bonded to the SiO_2 substrate over the sensing region for reagent handling. The graphene conducting channel was then biochemically functionalized. 1-Pyrenebutyric acid N-hydroxysuccinimide ester (PASE), which serves as a linker between the graphene and aptamer, was noncovalently coupled to the graphene via π–π interactions. IgE aptamer terminated with an amino group was attached to the PASE linker through N-hydroxysuccinimide (NHS) chemistry (Fig. 1d). Further details of the device fabrication and surface biochemical functionalization are provided in Fig. S2 in SI. A packaged GFET sensor is shown in Fig. 1e.

2.4 Measurements

The fabricated device was connected to a sourcemeter (Keithley 2400, Tektronix), providing both the drain and gate voltages. The drain current I_{ds} at appropriate V_{ds} and V_g was recorded throughout the experiment using a PC-based LabVIEW program. All experiments were performed in phosphate-buffered saline (PBS). Association of the protein and aptamer was initiated by introducing IgE solution to the aptamer functionalized graphene surface until I_{ds} reached an equilibrium state, after which fresh buffer was introduced to start the dissociation of the aptamer-IgE complex. IgE and buffer solutions were driven at a flow rate of 5 μL/min through the PDMS channel over the sensor surface, allowing binding measurements in flow-through mode. The temperature of the sensor was controlled through a closed-loop control system equipped with a Peltier plate and an embedded on-chip temperature sensor near the graphene sensing region (see Fig. 5a below and Fig. S6 in SI).

3. Results and Discussion

3.1 Surface Characterization

Raman spectroscopy was used to characterize the quality of the graphene and to determine if the surface modification with PASE and aptamers was successful. Prior to the chemical functionalization, the graphene channel between source and drain electrodes was initially characterized with Raman spectroscopy under 532 nm excitation. Obtained Raman spectra of the graphene channel exhibited a 2D band at ~2685 cm^{-1} and a G band at ~1588 cm^{-1} which are signatures of graphene (Fig. 2a) and shared by all graphitic sp^2 materials. However, the layer-dependent ratio of the intensity of the 2D band to the G band (I_{2D}/I_G) was 3.6, which provided further evidence of a single-layer graphene at this channel.[15] The attachment of PASE to the graphene surface split the pre-PASE G band located at 1588 cm^{-1} into two bands at 1587 cm^{-1} and 1626 cm^{-1}, confirming the coupling of graphene and pyrene groups on the PASE.[16] Also, the presence of D band located at 1342 cm^{-1} was observed, which was believed to be due to disordered carbon structure resulting from the graphene-PASE coupling. In addition, the 2D band shifted to a higher wavenumber (from 2679

to 2684 cm^{-1}), likely due to chemical doping resultant from the functionalization.

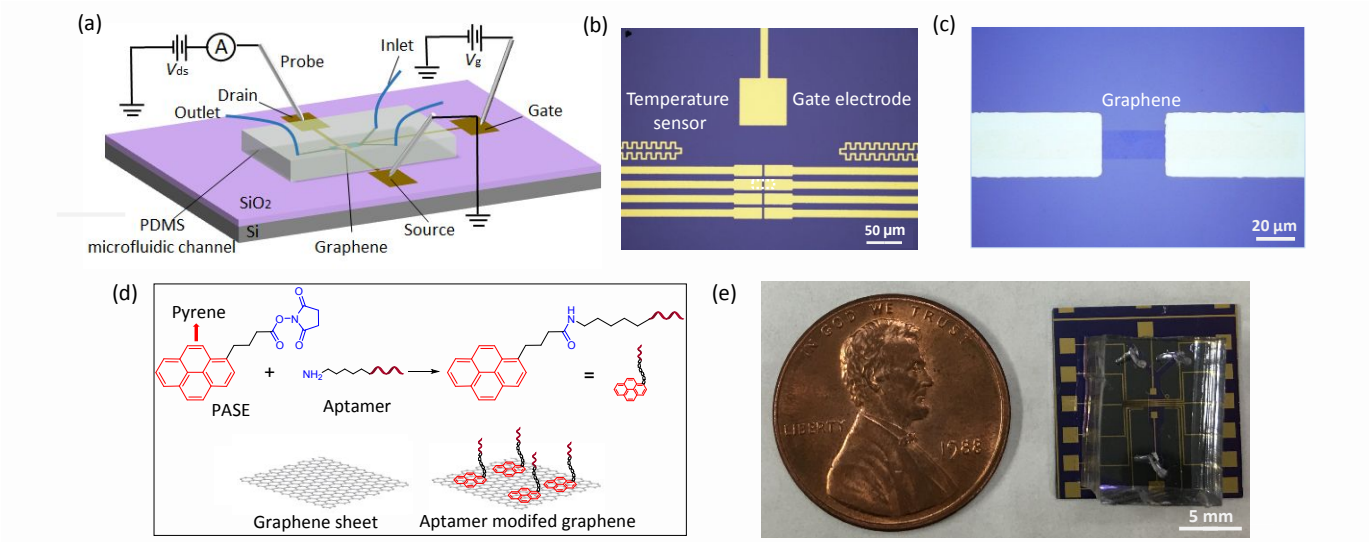

Fig. 1 (a) Schematic of the graphene nanosensor. The nanosensor is configured as an electrolyte-gated graphene field effect transistor, and is integrated with a PDMS microfluidic channel for reagent handling. (b) Micrograph of a fabricated device with an integrated gate electrode and temperature sensor. (c) Micrograph of the patterned graphene sensing region connecting drain and source electrodes. (d) Graphene surface immobilization. PASE is coupled to the graphene surface via π–π stacking and then the aptamer is attached to PASE through the formation of an amide group. (e) Packaged graphene nanosensor.

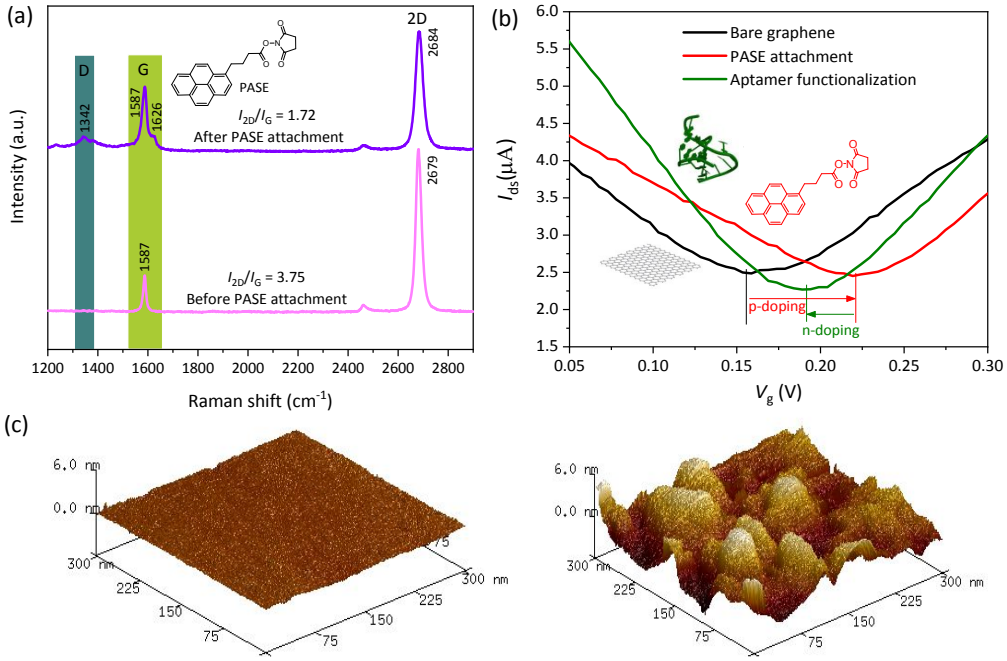

Fig. 2 Characterization of graphene surface functionalization. (a) Raman spectra, (b) Transport characteristic curve and (c) AFM image of graphene channel before and after PASE and aptamer attachment.

We further investigated the functionalization-induced doping by measuring the transport characteristic curve of the graphene sheet before and after PASE coupling; a shift in the V_{Dirac} (V_g when the drain current I_{ds} reached its minimum) from 158.2 mV to 221 mV (Fig. 2b) was observed, suggesting p-type doping. It is important to note that while the pyrene group of PASE is electron-rich and not predicted to induce p-type doping to the graphene, the carbonyl group of PASE is an electron-withdrawing group that can cause electron transfer from graphene to the linker molecule.[17] Transport characteristics were also used to confirm the functionalization of the PASE-modified graphene surface with aptamer molecules. Upon functionalization with aptamer molecules, V_{Dirac} left-shifted from

221 to 189.3 mV, suggesting n-type doping from the functionalization process. This can be explained by negatively-charged DNA strands serving as electron donors when interacting with graphene.[5] The surface immobilization was finally validated by analyzing the graphene surface topography before and after surface treatment via Atomic Force Microscope (AFM). The height of the graphene conducting channel from the substrate surface increased by ~ 3 nm (Fig. 2c), which was in agreement with reported aptamer thickness values on graphene.[18]

3.2 Determination of Binding Kinetics from Measurement Data

Interactions of the D17.4 aptamer with the IgE protein in PBS buffer were measured using the GFET nanosensor. An IgE concentration with a concentration of 5 nM was used in all experiments. The standard measurement conditions included temperature at 20 °C and PBS buffer containing 1 mM KH_2PO_4, 3 mM Na_2HPO_4 and 155 mM NaCl, added with 1 mM $MgCl_2$. In the experiments, IgE solution was injected through the PDMS microfluidic channel over the aptamer surface. The time-resolved sensor signal, i.e., drain current I_{ds} (t) (with t the time at the initiation of the flow of IgE solution), was measured to record the association process, in which IgE bound to the aptamer. After the association process sufficiently approached equilibrium with the drain current attaining a maximum saturation value ($I_{ds,max}$), the fluid in the PDMS microfluidic channel was replaced with pure PBS buffer to start the dissociation of IgE from the aptamer, which was again measured with the time-resolved sensor signal (Fig. 3).

Analysis of the measurement data was performed using a normalized sensor signal defined by:

$$y = \Delta I_{ds} / \Delta I_{ds,max} \quad (1)$$

where $\Delta I_{ds} = I_{ds}(t) - I_{ds}(0)$, and $\Delta I_{ds,max} = I_{ds,max} - I_{ds}(0)$. This normalized sensor signal was a measure of the density of aptamer-protein complexes on the sensor surface. Representative measurement data are shown in Fig. 3. The sensor signal was observed to increase monotonically in the association process until reaching a maximum value, and then decrease monotonically as IgE dissociated from the surface-immobilized aptamer. The error bars, representing standard deviations obtained from measurements using three devices, were considered small, indicating a low variability in the properties of the devices and in the aptamer-protein binding characteristics.

Assuming 1:1 aptamer-IgE binding and neglecting limitations of diffusion effects, the kinetics of the aptamer-protein binding measurements in flow-through mode can be mathematically mode led below.[19-22] The association process was represented by

$$y = y_\infty (1 - e^{-(k_{on}c + k_{off})t}) \quad (2)$$

and the dissociation processes by

$$y = e^{-k_{off}(t - t_d)} \quad (3)$$

In these equations, y_∞ is the asymptotic value of y if the association process extended to infinite time, t_d is the time when the dissociation process was initiated, and c is the protein concentration. In addition, k_{on} and k_{off} are respectively the association and dissociation rate constants of the aptamer-protein binding system, which are related to the equilibrium dissociation constant by

$$K_d = k_{off} / k_{on} \quad (4)$$

Note that y_∞ in eq. (1) is expected to slightly exceeds unity, and y = 1 at time $t = t_d$ by construction of the normalization method, eq (1).

To analyze the measured time history of the normalized sensor signal (e.g., Fig. 3), eqs. (2) and (3) were respectively fitted to the association ($0 \le t \le t_d$) and dissociation ($t \ge t_d$) profiles to obtain the association and dissociation constants, which were then used to calculate the equilibrium dissociation constant. The data fitting was performed using GraphPad Prism software (GraphPad Software, San Diego, CA).

Applying this analysis procedure to the data in Fig. 3 yielded k_{on} = 3.31 × 10^5 $M^{-1}s^{-1}$, k_{off} = 4.03 × 10^{-3} s^{-1}, and K_d = 12.15 nM. These kinetic binding parameters will be used as a basis of comparison in our subsequent studies of the effects of temperature and ionic strength on aptamer-protein binding kinetics. Also, the kinetic time constants were used to determine the time constants for the aptamer-protein association (176 s) and dissociation (248 s) processes. The electrical response of the graphene nanosensor (70 ms), as determined from the response time of the sensor due to a sudden gate voltage change (Fig. S3), in comparison, was three orders of magnitude smaller and hence was sufficiently fast to allow accurate measurements of aptamer-protein binding kinetics.

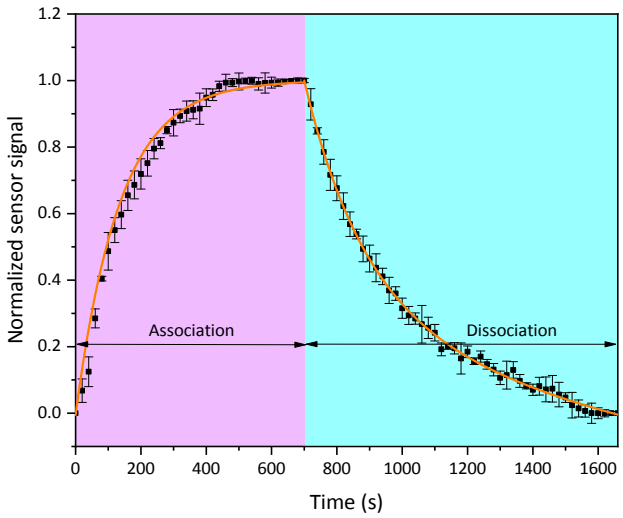

Fig. 3 Characterization of the kinetics of aptamer-IgE binding using the GFET nanosensor in PBS buffer containing 1 mM Mg^{2+} and 161 mM Na^+ at 20 ℃. Points are averages with error bars representing standard deviations from triplicate measurements.

3.3 Effects of Ionic Strengths on Aptamer-IgE Binding Kinetics

The effects of ionic strengths on the aptamer-IgE binding kinetics were investigated by varying the concentration of either Mg^{2+} or Na^+ from the standard-condition value. First, the Mg^{2+} concentration was varied from the standard-condition value (1 mM) by adding $MgCl_2$ into the buffer, with the Na^+ concentration (161 mM) and temperature (20 °C) unchanged (Fig. 4a). The association rate constant k_{on} increased from 3.31 × 10^5 to 2.05 × 10^7 $M^{-1}s^{-1}$ and the dissociation rate constant k_{off} from 4.03 × 10^{-3} to 18.68 × 10^{-3} s^{-1} when the Mg^{2+} concentration increased from 1 to 40 mM. The

obtained association rate constant k_{on} and dissociation rate constant k_{off} resulted in a decrease in the equilibrium dissociation constant K_d from 12.15 to 0.9 nM (Table 1) with increasing Mg^{2+} concentration.

Next, the Na^+ concentration was varied from the standard-condition value (161 mM) by adding NaCl into the buffer, with the Mg2+ concentration (1 mM) and temperature (20 °C) unchanged (Fig. 4b). The association rate constant k_{on} was found to increase from 3.31×10^5 to 8.42×10^6 $M^{-1}s^{-1}$, and the dissociation rate constant k_{off} increased from 4.03×10^{-3} to 3.42×10^{-2} s^{-1}. This resulted in a decrease in the dissociation constant K_d from 12.15 to 4.05 nM while the Na^+ concentration increased from 161 to 450 mM (Table 2). The association and dissociation profiles showed that both association and dissociation rate constants increased with increasing concentrations of Na^+ and Mg^{2+} ions. Generally, the strong electrostatic interaction between salts ions and the negatively charged backbone of DNA strands pre-fold the aptamer, and higher salt concentrations may fold the aptamer into a more favorable configuration for ligand-receptor recognition.[23, 24] In contrast, it has been revealed that a major effect of salt-dependent dissociation is the re-condensation of cations on DNA upon dissociation. Under these conditions, the higher salt concentration increases the dissociation.[25] The equilibrium dissociation constant K_d of aptamer-IgE interaction resulted from increased Na^+ and Mg^{2+} levels was found to decrease, suggesting that the salt ions generally improved the binding affinity of the protein and aptamer. Nevertheless, it was seen that an increase in Mg^{2+} concentration from 1 to 40 mM caused the dissociation constant K_d to drop by 13.5 times from 12.15 to 0.9 nM. In comparison, a larger increase in Na^+ concentration (from 161 to 450 mM) resulted in a considerably smaller decrease in K_d (by 3 times from 12.15 to 4.05 nM). This could be attributed to divalent cations (e.g., Mg^{2+}) producing a larger change of aptamer conformational structure than monovalent cations (e.g., Na^+).[26] Furthermore, for the concentration range measured, the dissociation constant K_d depended approximately linearly on Na^+ concentration at a rate of 0.027 nM/mM (Fig. S4a). In contrast, for the concentration range tested, increased Mg^{2+} concentration caused a strong nonlinearity in the dissociation constant (Fig. S4b), which likely suggests a larger conformational structure change of the aptamer when interacting with Mg^{2+}.

Predicted secondary structures of the IgE aptamer at increased Mg^{2+} concentration using mfold (The RNA Institute, Albany, NY) exhibits a change in the conformational structure from a single stem-loop to a two-stem-loop conformation (Fig. S5). In contrast, the secondary structure predictions of the aptamer remained the same for our experimental range of Na^+. Thus, we hypothesize that the prominent mechanism of Mg^{2+}-dependent binding kinetics is likely the conformational change of the aptamer when interacting with Mg^{2+}, while electrostatic interaction is the main contributor to the dependence of binding kinetics on Na^+. Interestingly, at very high salt ionic strength (450 mM), the binding interactions between the IgE and aptamer molecules could be observed despite the short Debye screening length, a length that describes a charge carrier's net electrostatic effect in electrolytes.[26] At this concentration, it was predicted that the Debye length is less than 0.7 nm[27] that is lower than the aptamer height (~3 nm). Therefore, the electrostatic gating effect generated by the charged IgE captured by the aptamer on the graphene surface is predicted to be relatively weak.

In addition to the electrostatic gating caused by IgE, there are two other possible contributors to the signal transduction. First, upon the capture of IgE, the aptamer experiences a larger change in the conformational structure which brings the electron-rich aromatic nucleotide strands into close proximity with the graphene surface, resulting in direct charge transfer between nucleotides and the graphene surface. The closer interactions make electrons from the IgE aptamer more likely to be directly transferred into the graphene. Second, captured target molecules can act as a second capacitor to the system, and this extra capacitance will be in series to the gating system that is formed at the graphene-electrolyte interface.[28] The magnitude of this capacitance will be dependent on the amount of target molecules captured on the graphene surface and therefore will influence the electrical conductivity of the graphene channel.

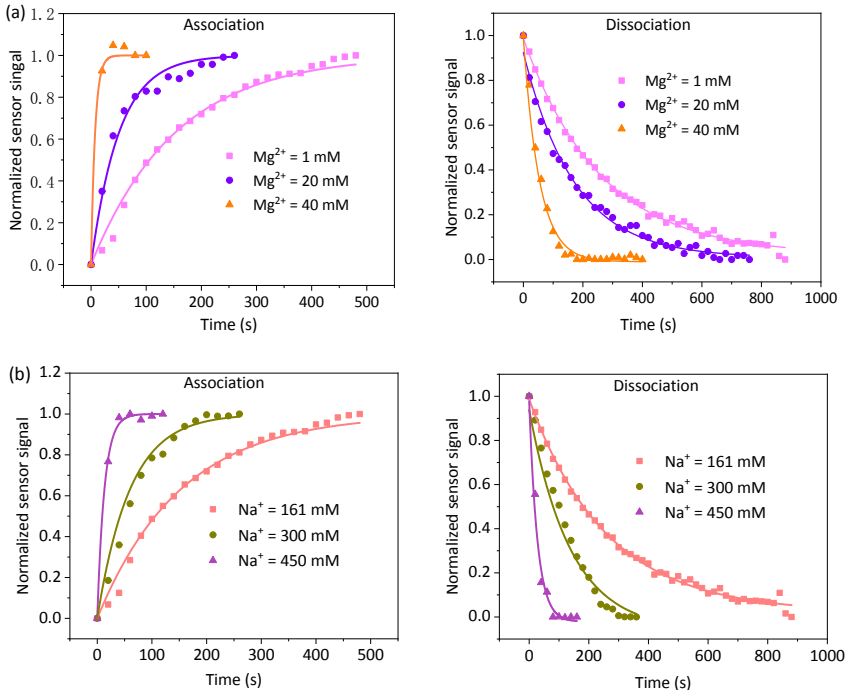

Fig. 4 Effects of Mg^{2+} and Na^{+} concentrations on aptamer-IgE association and dissociation kinetics. Association and dissociation profiles of the aptamer-IgE interaction at (a) different Mg^{2+} and (b) different Na^{+} concentrations.

Table 1 Characterization of aptamer-IgE binding at different Mg^{2+} concentrations

c_{Mg2+} (mM)	k_{off} (s^{-1})	k_{on} ($M^{-1}s^{-1}$)	K_d (nM)
1	4.03×10^{-3}	3.31×10^{5}	12.15
20	5.81×10^{-3}	3.46×10^{6}	1.68
40	1.87×10^{-2}	2.05×10^{7}	0.9

Table 2 Characterization of aptamer-IgE binding at different Na^{+} concentrations

c_{Na+} (mM)	k_{off} (s^{-1})	k_{on} ($M^{-1}s^{-1}$)	K_d (nM)
161	4.03×10^{-3}	3.31×10^{5}	12.15
300	7.20×10^{-3}	1.01×10^{6}	7.17
450	3.42×10^{-2}	8.42×10^{6}	4.05

3.4 Effects of Temperature on Aptamer-IgE Binding Kinetics

The temperature-dependent kinetics of the aptamer-IgE binding was studied by varying the temperature from the standard condition (20 °C) in a range of 10-32 ℃ via on-chip closed-loop temperature control (Fig. 5a). Details of the temperature control are given in SI (Figs. S7 and S8). While the association and dissociation processes both depend on temperature, we chose to focus on temperature-dependent dissociation to study the thermodynamic properties of aptamer-IgE binding. Dissociation profiles of the aptamer-IgE complex exhibited a strong temperature dependence (Fig. 5b). The results suggested that the increased temperature was prone to accelerate the dissociation, as the dissociation rate constant increased from 1.03×10^{-3} to 3.16×10^{-2} s^{-1} when the temperature rose from 10 to 32 ℃. Such a strong dependence can be explained by the progressive destabilization of the aptamer structure resultant from the increased temperature.[23] This characteristic allows temperature-mediated regeneration of the aptamer surface, where the captured target analyte can be released because of the conformational change of the aptamer which can then be recovered at lower temperatures.[29] We fitted the experimental results to the following Arrhenius equation shown in eq. (5) to determine the temperature-dependent reaction rates,[30]

$$\ln(k_{off}) = \frac{E_a}{RT} + \ln(A) \quad (5)$$

where k_{off} is the dissociation rate constant, E_a is the activation energy, T is the absolute temperature, R is the gas constant and A is the collision frequency factor. When $\ln(k_{off})$ and $1/T$ is plotted, E_a and A can be found by performing a linear fit and matching the slope and y-intercept to eq. (5) (Fig. 5c). Other transition-state thermodynamic parameters such as enthalpy change of activation ($\Delta H^{\#}$), entropy change of activation ($\Delta S^{\#}$) and free energy change of activation ($\Delta G^{\#}$) can then be determined from the following equations:

$$\Delta H^{\#} = E_a - RT \quad (6)$$

$$\Delta S^{\#} = R(\ln\frac{Ah}{k_B T} - 1) \quad (7)$$

$$\Delta G^{\#} = \Delta H^{\#} - T\Delta S^{\#} \quad (8)$$

where h is the Planck constant, R is the gas constant, and k_B is the Boltzmann constant. The thermodynamic parameters were calculated to be E_a = 20.49 kcal mol^{-1}, $\Delta H^{\#}$ = 19.90 kcal mol^{-1}, $\Delta S^{\#}$ = -0.89 cal $mol^{-1}k^{-1}$ and $\Delta G^{\#}$ = 20.16 kcal mol^{-1}. The results are found to reasonably agree with published data.[1] The discrepancy between our results and recent anisotropy results may be attributed to the slightly different ionic strength of buffers and differences in room temperature.

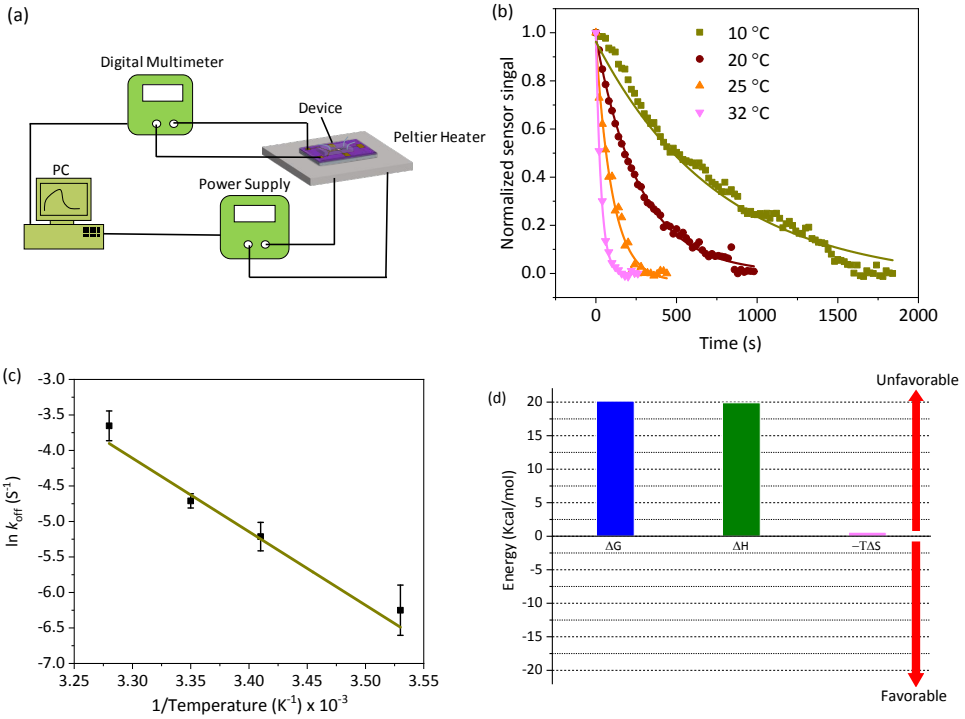

Fig. 5 Effects of temperature on aptamer-IgE dissociation kinetics. (a) Experimental setup. (b) Dissociation profiles at different temperatures. (c) Arrhenius plots for dissociation of aptamer-IgE complex as a function of temperature. Error bars are standard deviations from triplicate measurements. (d) Thermodynamic parameters for aptamer-IgE dissociation.

From a thermodynamic perspective, the dissociation of the aptamer-IgE complex is unfavorable both in entropy and enthalpy as plotted in Fig. 5d. The large unfavorable $\Delta H^{\#}$ for the complex dissociation, as the main component of $\Delta G^{\#}$, represents that the major barrier for the dissociation is mainly the breaking of noncovalent bonds between binding partners. It has been revealed that hydrogen bonds and Van der Waals contacts exist in complexes are directly proportional to the corresponding $\Delta H^{\#}$ values.[31] Thus, the large unfavorable $\Delta H^{\#}$ can be attributed to electrostatic interactions involved in aptamer-IgE complexes. On the other hand, we may attribute the negative unfavorable $\Delta S^{\#}$ to the re-condensation of ions onto the dissociated IgE, since this process is in reverse to aptamer-IgE association which involves releasing condensed ions causing a favorable entropic change.[1, 23]

4. Conclusions

Characterization of the kinetics and thermodynamics of biomolecular interactions has been performed using graphene nanosensing. The approach employed a graphene FET nanosensor with a fully integrated on-chip gate electrode, temperature sensor, and microfluidic flow cell. Binding between a protein and a specific aptamer immobilized on the graphene surface alters the electrical conductance of the graphene channel, which was measured in a time-resolved manner to characterize the binding kinetics. This approach was applied to the binding of human immunoglobulin E (IgE), used as a representative analyte, to the aptamer. Experimental results demonstrated that increased levels of salt ions or temperatures resulted in increased association and dissociation rates between IgE and aptamer. For Mg^{2+} ranging from 1 to 40 mM in concentration, the association rate constant increased from 3.31×10^5 to 2.05×10^7 $M^{-1}s^{-1}$, and the dissociation rate constant increased from 4.03×10^{-3} to 18.68×10^{-3} s^{-1}. For Na^+ ranging from 161 to 450 mM, the association rate constant increased from 3.31×10^5 to 8.42×10^6 $M^{-1}s^{-1}$, and the dissociation rate constant increased from 4.03×10^{-3} to 3.42×10^{-2} s^{-1}. As the temperature rose from 10 to 32 ℃, the dissociation rate constant increased from 1.03×10^{-3} to 3.16×10^{-2} s^{-1}. In addition, the kinetic dissociation constant was found to be correlated linearly with the Na^+ concentration, and related strongly nonlinearly to the Mg^{2+} concentration. This is consistent with the knowledge that divalent cations produce larger changes in the conformational structure of the aptamer than monovalent cations. The strong environmental dependence of the kinetics of aptamer-IgE binding provides insights into kinetic characteristics of aptamer-protein binding. These results demonstrate that GFET nanosensors can potentially be used as an innovative tool for direct, label-free, reliable, and systematic characterization of biomolecular interaction kinetics.

Conflicts of interest

The authors declare no conflicts in the work presented.

Acknowledgements

This work was support by National Science Foundation (Grant No. ECCS-1509760). X. Wang gratefully acknowledges a National Scholarship (Award No. 201406740003) from the China Scholarship Council. This work made use of instruments in the CNI cleanroom at Columbia University and the ASRC cleanroom at the City University of New York. The authors would also like to thank Mr. Z. Wang and Dr. S. Yu for discussions on kinetic binding modeling, and Mr. P. Spezza for proofreading the manuscript.

References

1 M. V. Poongavanam, L. Kisley, K. Kourentzi, C. F. Landes and R. C. Willson, *Biochim. Biophys. Acta, Proteins and Proteomics*, 2016, **1864**, 154-164.
2 C. Hahnefeld, S. Drewianka and F. W. Herberg, *Molecular Diagnosis of Infectious Diseases*, 2004, 299-320.
3 C. Wu, X. Li, S. Song, Y. Pei, L. Guo and Z. Pei, *Polymers*, 2017, **9**, 482.
4 K. S. Novoselov, A. K. Geim, S. Morozov, D. Jiang, Y. Zhang, S. a. Dubonos, I. Grigorieva and A. Firsov, *Science*, 2004, **306**, 666-669.
5 X. Dong, Y. Shi, W. Huang, P. Chen and L. J. Li, *Adv. Mater.*, 2010, **22**, 1649-1653.
6 Y.-M. Lin and P. Avouris, *Nano Lett.*, 2008, **8**, 2119-2125.
7 V. Georgakilas, M. Otyepka, A. B. Bourlinos, V. Chandra, N. Kim, K. C. Kemp, P. Hobza, R. Zboril and K. S. Kim, *Chem. Rev.*, 2012, **112**, 6156-6214.
8 C. Zheng, L. Huang, H. Zhang, Z. Sun, Z. Zhang and G.-J. Zhang, *ACS Appl. Mater. Inter.*, 2015, **7**, 16953-16959.
9 Z. Hao, Y. Pan, W. Shao, Q. Lin and X. Zhao, *Biosens. Bioelectron.*, 2019, **134**, 16-23.
10 S. Afsahi, M. Lerner, J. M. Goldstein, J. Lee, X. Tang, D. A. Bagarozzi, D. Pan, L. Locascio, A. Walker, F. Barron and B. R. Goldsmith, *Biosens. Bioelectron.*, 2018, **100**, 85-88.
11 L. Zuccaro, C. Tesauro, T. Kurkina, P. Fiorani, H. K. Yu, B. R. Knudsen, K. Kern, A. Desideri and K. Balasubramanian, *ACS Nano*, 2015, **9**, 11166-11176.
12 J. E. Schiel and D. S. Hage, *J. Sep. Sci.*, 2009, **32**, 1507-1522.
13 S. Xu, J. Zhan, B. Man, S. Jiang, W. Yue, S. Gao, C. Guo, H. Liu, Z. Li, J. Wang and Y. Zhou, *Nat. Commun.*, 2017, **8**, 14902.
14 Y. N. Kosaganov, D. A. Stetsenko, E. N. Lubyako, N. P. Kvitko, Y. S. Lazurkin and P. E. Nielsen, *Biochemistry*, 2000, **39**, 11742-11747.
15 X. Li, W. Cai, J. An, S. Kim, J. Nah, D. Yang, R. Piner, A. Velamakanni, I. Jung and E. Tutuc, *Science*, 2009, **324**, 1312-1314.
16 X. Wang, Y. Zhu, T. R. Olsen, N. Sun, W. Zhang, R. Pei and Q. Lin, *Phys. Electrochim. Acta,* 2018, **290**, 356-363.
17 Y. Zhu, Y. Hao, E. A. Adogla, J. Yan, D. Li, K. Xu, Q. Wang, J. Hone and Q. Lin, *Nanoscale*, 2016, **8**, 5815-5819.
18 C. Wang, J. Kim, Y. Zhu, J. Yang, G.-H. Lee, S. Lee, J. Yu, R. Pei, G. Liu and C. Nuckolls, *Biosens. Bioelectron.*, 2015, **71**, 222-229.
19 L. C. James and D. S. Tawfik, *P. Natl. Acad. Sci.*, 2005, **102**, 12730-12735.
20 R. Yu and Y. Cao, *Sci. Rep.*, 2017, **7**, 13279.
21 I. Fakih, S. Sabri, F. Mahvash, M. Nannini, M. Siaj and T. Szkopek, *Appl. Phys. Lett.*, 2014, **105**, 083101.
22 X. Pang and H. Zhou, *Annu. Rev. Biophys.*, 2017, **46**, 105-130.
23 I. Kanakaraj, W.-H. Chen, M. Poongavanam, S. Dhamane, L. J. Stagg, J. E. Ladbury, K. Kourentzi, U. Strych and R. C. Willson, *Int.*

J. Biol. Macromol., 2013, **57**, 69-75.
24 A. S. Potty, K. Kourentzi, H. Fang, P. Schuck and R. C. Willson, *Int. J. Biol. Macromol.*, 2011, **48**, 392-397.
25 T. M. Lohman and P. H. von Hippel, *Crit. Rev. Biochem. Mol. Biol.*, 1986, **19**, 191-245.
26 S. Sorgenfrei, C.-Y. Chiu, M. Johnston, C. Nuckolls and K. L. Shepard, *Nano Lett.*, 2011, **11**, 3739-3743.
27 E. Stern, R. Wagner, F. J. Sigworth, R. Breaker, T. M. Fahmy and M. A. Reed, *Nano Lett.*, 2007, **7**, 3405-3409.
28 G. Palazzo, D. De Tullio, M. Magliulo, A. Mallardi, F. Intranuovo, M. Y. Mulla, P. Favia, I. Vikholm - Lundin and L. Torsi, *Adv. Mater.*, 2015, **27**, 911-916.
29 J. Zhu, T. Nguyen, R. Pei, M. Stojanovic and Q. Lin, *Lab Chip*, 2012, **12**, 3504-3513.
30 K. A. Xavier and R. C. Willson, *Biophys. J.*, 1998, **74**, 2036-2045.
31 J. Kang and J. D. Auerbach, *Mol. Immunol.*, 2009, **46**, 2873-2875.

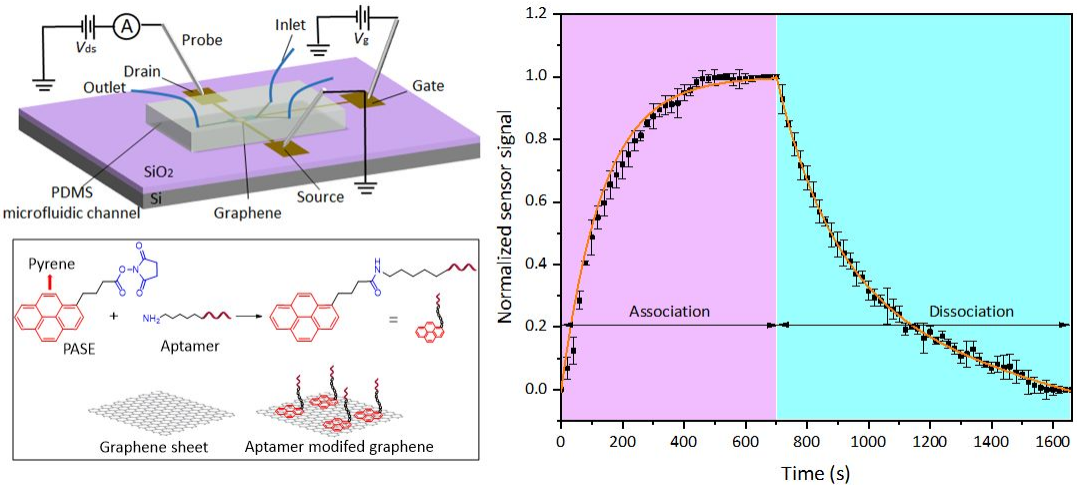

Measurements of Aptamer-Protein Binding Kinetics Using Graphene Field-Effect Transistors